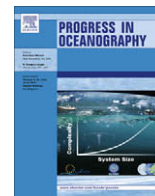




Contents lists available at ScienceDirect

Progress in Oceanography

journal homepage: www.elsevier.com/locate/pocean

Preliminary forecasts of Pacific bigeye tuna population trends under the A2 IPCC scenario

P. Lehodey^{a,*}, I. Senina^a, J. Sibert^b, L. Bopp^c, B. Calmettes^a, J. Hampton^d, R. Murtugudde^e

^a MEMMS (Marine Ecosystems Modelling and Monitoring by Satellites), CLS Satellite Oceanography Division, Ramonville, France

^b PFRP (Pelagic Fisheries Research Program), University of Hawaii at Manoa, Honolulu, HI, USA

^c LSCE/IPSL, UMR 1572 CE Saclay, Gif sur Yvette, France

^d Oceanic Fisheries Programme, Secretariat of the Pacific Community, Noumea, New Caledonia

^e ESSIC, Earth Science System Interdisciplinary Center, University of Maryland, USA

ARTICLE INFO

Article history:

Received 20 March 2008

Received in revised form 10 November 2009

Accepted 10 April 2010

Available online 20 April 2010

ABSTRACT

An improved version of the spatial ecosystem and population dynamics model SEAPODYM was used to investigate the potential impacts of global warming on tuna populations. The model included an enhanced definition of habitat indices, movements, and accessibility of tuna predators to different vertically migrant and non-migrant micronekton functional groups. The simulations covered the Pacific basin (model domain) at a $2^\circ \times 2^\circ$ geographic resolution. The structure of the model allows an evaluation from multiple data sources, and parameterization can be optimized by adjoint techniques and maximum likelihood using fishing data. A first such optimized parameterization was obtained for bigeye tuna (*Thunnus obesus*) in the Pacific Ocean using historical catch data for the last 50 years and a hindcast from a coupled physical–biogeochemical model driven by the NCEP atmospheric reanalysis. The parameterization provided very plausible biological parameter values and a good fit to fishing data from the different fisheries, both within and outside the time period used for optimization. We then employed this model to forecast the future of bigeye tuna populations in the Pacific Ocean. The simulation was driven by the physical–biogeochemical fields predicted from a global marine biogeochemistry – climate simulation. This global simulation was performed with the IPSL climate model version 4 (IPSL–CM4) coupled to the oceanic biogeochemical model PISCES and forced by atmospheric CO₂, from historical records over 1860–2000, and under the SRES A2 IPCC scenario for the 21st century (i.e. atmospheric CO₂ concentration reaching 850 ppm in the year 2100). Potential future changes in distribution and abundance under the IPCC scenario are presented but without taking into account any fishing effort. The simulation showed an improvement in bigeye tuna spawning habitat both in subtropical latitudes and in the eastern tropical Pacific (ETP) where the surface temperature becomes optimal for bigeye tuna spawning. The adult feeding habitat also improved in the ETP due to the increase of dissolved oxygen concentration in the sub-surface allowing adults to access deeper forage. Conversely, in the Western Central Pacific the temperature becomes too warm for bigeye tuna spawning. The decrease in spawning is compensated by an increase of larvae biomass in subtropical regions. However, natural mortality of older stages increased due to lower habitat values (too warm surface temperatures, decreasing oxygen concentration in the sub-surface and less food). This increased mortality and the displacement of surviving fish to the eastern region led to stable then declining adult biomass at the end of the century.

© 2010 Elsevier Ltd. All rights reserved.

1. Introduction

Climate warming simulations have been conducted for more than a decade using different coupled Atmosphere–Ocean General Circulation Models (AOGCMs) to investigate the response of the physical atmosphere–ocean system to increased greenhouse gases and aerosols (Cubasch et al., 2001; IPCC, 2007). Physical changes

* Corresponding author. Tel.: +33 561 393 782; fax: +33 561 393 770.
E-mail address: plehodey@cls.fr (P. Lehodey).

predicted from these simulations, i.e., warming, changes in cloudiness and mixed layer thickness, and increased vertical stratification, very likely will cause significant adjustments in the biology of the oceans (Denman et al., 1996; Cox et al., 2000; Bopp et al., 2001; Boyd and Doney, 2002). In particular, higher stratification is predicted to reduce nutrient supply while warming and changes in cloudiness affect photosynthesis directly. Nevertheless, global warming impacts would result in large regional variability.

Using six of these AOGCM simulations, Sarmiento et al. (2004) investigated the ocean biological response to global warming,

between the beginning of industrial period and 2050, with a diagnostic model of primary production (PP) based on the definition of large ocean biomes. At global scales, the simulations predict an increase in primary production in the range of 0.7–8.1%. This high level of aggregation integrates large regional differences: a contraction of the highly productive marginal sea ice biome (–42% in the Northern Hemisphere and –17% in the Southern Hemisphere), an expansion of the low productivity permanently stratified subtropical gyre biome (+4.0% in the Northern Hemisphere and +9.4% in the Southern Hemisphere), a spatial expansion of the subpolar gyre biome (+16% in the Northern Hemisphere and +7% in the Southern Hemisphere), and a contraction of the seasonally stratified subtropical gyres (–11% in both hemispheres). The low-latitude (mostly coastal) upwelling biome area changes only modestly.

Another approach to explore the impact of global warming on ocean primary productivity is to couple AOGCMs to mechanistic biogeochemical models (e.g. Fasham et al., 1990; Sarmiento et al., 1993; Aumont et al., 1999; Bopp et al., 2001; Christian et al., 2002). A recent comparison of observations with simulation outputs from three of such coupled models (IPSL, MPIM, NCAR) showed good agreement between independent estimates from coupled models and satellite observations (Schneider et al., 2008), providing increased confidence that such models can help in studying the impact of global warming on marine productivity and carbon export. Results from these coupled models reproduce the chain of cause and effect leading from stratification through nutrient concentrations to primary production. They confirmed the role of the low-latitude, permanently stratified ocean for global primary production anomalies (Behrenfeld et al., 2006). In particular, the IPSL model is able to reproduce the observed relationship between interannual variability in climate (e.g., change in stratification and SST) and primary production. It predicts that the PP would decrease under the possible more El Niño-like conditions with surface warming and stronger stratification in the equatorial region. For example, an increase of the average SST of 1.6 °C between 2000 and 2100 under the IPCC A2 scenario would reduce PP in the equatorial region by 9%.

Here, we used outputs from this IPSL coupled model as the forcing of an improved version of the spatial ecosystem and population dynamics model SEAPODYM (Lehodey et al., 2008; Senina et al., 2008). We employed this model to forecast the future of bigeye tuna (*Thunnus obesus*) populations in the Pacific Ocean under the SRES A2 IPCC scenario for the 21st century (i.e., atmospheric CO₂ concentrations reaching 850 ppm in the year 2100, and historical data between 1860 and 2000).

Bigeye tuna has an extended habitat in the three oceans, from the equator to temperate regions. The species has a life-span >10 years, age at first maturity between 2 and 3 years and spawning occurs in tropical warm waters. While young fish are found in surface schools with other tuna species (skipjack [*Katsuwonus pelamis*] and yellowfin [*Thunnus albacares*]), the adults explore deeper layers where they can find mesopelagic prey species. These deep excursions are made possible by their highly specialized physiology. In particular, they have a well developed 'rete mirabile', that is a counter-current heat exchange system in the red muscle, and a good tolerance to low dissolved oxygen concentration. Bigeye tuna is a very valuable species and is facing high fishing pressure from the longline sub-surface fisheries, but also as by-catch of purse seine surface tuna fisheries.

Here, we present the approach that was followed to parameterize and evaluate the model using historical fishing data. Then, a simulation was conducted with the IPSL forcing to forecast the physical and biogeochemical changes in the Pacific Ocean under the A2 IPCC scenario.

2. Materials and methods

To establish confidence in the forecast of the model SEAPODYM under the IPCC climate change forcing, our first objective was to evaluate the prediction of the model for the historical and present periods. Thus, existing data and independent estimates of species biomass can be used to assess the model outputs. In addition, it was essential to check the model prediction outside of the time window used for the parameters optimization, to verify that the mechanisms included in the model are robust and sufficient to predict species dynamics and the observed historical catch. Therefore, the analysis consisted of three steps: (i) model parameters optimization using fishing data for the recent period (1985–2000), (ii) hindcast simulation for the period 1965–1985 with the estimated parameters and (iii) the forecast experiment (2001–2100). The forcing fields used for these different experiments were obtained from the ESSIC-coupled ocean-biogeochemical model driven by the atmospheric NCEP reanalysis, and the IPSL Earth Climate change simulation.

2.1. SEAPODYM

SEAPODYM is a model developed initially for investigating spatial tuna population dynamics under the influence of both fishing and environmental effects (Lehodey et al., 2003). The model is based on advection–diffusion–reaction equations. The main features of this model are: (i) forcing by environmental data (temperature, currents, primary production and dissolved oxygen concentration), (ii) prediction of both temporal and spatial distribution of mid-trophic (micronektonic tuna forage) functional groups, (iii) prediction of both temporal and spatial distribution of age-structured predator (tuna) populations, (iv) prediction of total catch and size frequency of catch by fleet when fishing data (catch and effort) are available, and (v) parameter estimation based on fishing data assimilation techniques (see below, and Senina et al., 2008).

A recent enhanced version (Lehodey et al., 2008) has been developed that includes a better definition of habitat indices, movements, and accessibility of tuna and tuna-like predators to different vertically migrant and non-migrant micronekton functional groups (Lehodey et al., 2010). These groups are represented in a three-layer vertical environment delineated using predicted euphotic depth that is used to achieve a more realistic vertical structure of pelagic ecosystem. Thus, the epipelagic layer is between surface and 1× euphotic depth, the mesopelagic layer between 1× and 3× the euphotic depth and the bathypelagic layer between 3× the euphotic depth and 1000 m. Temperature, zonal (*u*) and meridional (*v*) currents and dissolved oxygen predicted from ocean physical–biogeochemical simulations are averaged following this definition of layers while total primary production is integrated over the entire vertical layer. This new definition of vertical layers was used with the IPSL simulation, while the parameter estimation for bigeye tuna using ESSIC hindcast followed the same model configuration as the one used for Pacific skipjack tuna as described in Senina et al. (2008), i.e. constant depth layers.

2.2. NCEP–ESSIC Pacific Ocean simulation

Forcing fields derived from the NCEP–ESSIC simulation covering the period 1948–2004 on a monthly 2° × 2° resolution were described in Lehodey et al. (2008), Senina et al. (2008) and Lehodey et al. (2010), where they were used to drive simulations of skipjack and bigeye tunas and their mid-trophic level prey organisms. The ESSIC model simulation is driven by 2D atmospheric fields (NCEP) and provides reasonable predictions of interannual and interdecadal variability. In particular, all ENSO events are well reproduced as

well as the mid-1970s regime shift (Wang et al., 2005, 2006). However, the model was developed and parameterized for tropical oceans and the seasonality at high latitudes presents some bias (see Section 2.3.). In addition, the model did not predict dissolved oxygen concentration so we used quarterly climatological data (Garcia et al., 2006).

2.3. IPSL–PISCES Earth Climate simulation

The IPSL–PISCES Earth Climate simulation provided physical–biogeochemical fields used to drive SEAPODYM and to investigate the responses of bigeye tuna population dynamics to global warming. The IPSL climate model (Marti et al., 2006) is composed of an oceanic physical component OPA, a sea ice component LIM, an atmospheric component LMDZ, and a land surface component ORCHIDEE, coupled through the OASIS coupler. The global climate simulation starts with climatological conditions and the only variable forcing is the change in atmospheric CO₂ concentration. The simulation uses the historical atmospheric CO₂ concentration between 1860 and 2000, which then increases according to the SRES A2 IPCC scenario for the 21st century, i.e., atmospheric CO₂ concentrations reaching 850 ppm in the year 2100. Physical forcing fields from the climate simulation have then been used to force an offline version of the oceanic biogeochemical model PISCES (for Pelagic Interactions Scheme for Carbon and Ecosystem Studies; Aumont and Bopp, 2006) over a similar period (1860–2100) and for the global ocean. PISCES incorporates both multi-nutrient limitation (NO₃, NH₄, PO₄, SiO₃ and Fe) and a description of the plankton community structure with four plankton functional groups (diatoms, nano-phytoplankton, micro-zooplankton and meso-zooplankton). A detailed description and evaluation of those simulations is provided in Bopp et al. (2005) and Schneider et al. (2008).

These simulations reproduce the seasonal cycle reasonably well and the atmosphere–ocean coupled system generates internal variability at interannual to interdecadal frequencies. However, while ocean simulations that are forced by observation-derived wind fields (e.g. NCEP atmospheric reanalysis) lead to realistic interannual to decadal variability, the ones produced by climate models are not expected to be in phase with the actual observed variability. To illustrate these differences, we compared the predicted outputs of the ESSIC simulation with the IPSL–PISCES simulation and observations.

2.4. Parameter estimation

The parameter optimization method is fully described in Senina et al. (2008) and will only be briefly mentioned here. SEAPODYM produces estimates of total catch and catch by size based on model calculations of age-structured population abundance and other variables and observed data on fishing effort. The maximum-likelihood approach uses a joint-likelihood function consisting of contributions from discrepancies in total catches and catches by size (see Appendix A). The maximum is found by minimizing the negative logarithm of likelihood using a quasi-Newton numerical function minimization algorithm and gradients computed using adjoint functions. The standard deviations of all estimated parameters were computed in the vicinity of the optimum from the inverse Hessian matrix (Bard, 1974). The Hessian matrix was approximated by central finite differences using first derivatives exactly evaluated by adjoint calculations.

The parameterization that has been obtained from the ESSIC simulation cannot be applied directly to the IPSL simulation because of significant differences in the forcing fields. The ESSIC hindcast was based on a previous definition of vertical layers, with fixed boundaries of 0–100 m, 100–400 m and 400–1000 m for epipe-

lagic, mesopelagic and bathypelagic layers respectively, while in the new version used with IPSL climate simulation, the vertical boundaries were defined in relation to the euphotic depth. In addition, dissolved oxygen fields used with the ESSIC forcing fields were those from the seasonal Levitus climatology (Garcia et al., 2006), while in the IPSL–PISCES experiment the concentration of oxygen is directly computed in the model.

Because of these differences in the configuration of simulations, it was necessary to test the sensitivity of parameters estimated with the first optimization experiment (i.e. forced by ESSIC) to the new forcing field of the IPSL simulation. Thus, we conducted a series of simulations with optimal parameters estimated from actual fishing data in the Pacific Ocean for the recent period 1985–2000 and the physical–biogeochemical fields of the IPSL simulation, and compared results with those of the ESSIC-based optimization.

To evaluate the model's ability to capture the essential features of the dynamics of the bigeye tuna population, we carried out a hindcast simulation back to the early 1960s, i.e. the beginning of industrial fishing, with the fixed “best-parameterization” achieved from optimization experiments, and compared predicted catches conditioned on the observed fishing effort and observed catches. Bigeye tuna biomass trends were also compared to those estimated from a state-of-the-art standard stock-assessment model used by the Western Central Pacific Fisheries Commission. Then we used the model framework for the entire period (1860–2100), without fishing effort, to investigate the general trends of biomass and spatial distributions associated with environmental changes under the increasing forcing of atmospheric CO₂.

3. Results

3.1. Forcing fields

Before comparing the results of the two optimization experiments, it was critical to examine differences in the forcing fields of the two simulations. The euphotic depth was of particular importance since it defines the three vertical layers in the enhanced version of SEAPODYM used in IPSL-forced experiments, and within which physical variables (temperature, currents) and oxygen content were averaged. While the epipelagic layer coincides with the euphotic depth in the IPSL-forced experiment, it was fixed to 100 m in the previous ESSIC-forced experiment.

Euphotic depth is strongly inversely correlated with primary production and can be empirically deduced from chlorophyll-*a* satellite data (Morel and Berthon, 1989). Euphotic depth calculated from SeaWiFS chlorophyll data¹ is shown on Fig. 1 for three large geographical regions influenced by the main climate variability of the period used for optimization, i.e. seasonal and interannual (ENSO) signals. On average, the values of Z_{eu} of both satellite-derived (VGPM) and model (IPSL) series are in the same range in the equatorial regions (cold tongue and warm pool), i.e. ~80–100 m, but the IPSL simulation predicted a stronger seasonal variability at higher latitudes (North Pacific) with a shallower depth peaking in May–June (~50 m) while shallowest SeaWiFS-derived euphotic depth (80 m) occurred in April.

Average series of temperature in the epipelagic layers and vertically integrated PP predicted by the ESSIC hindcast and IPSL climate simulation (Fig. 2) are compared to the temperature predicted by the SODA reanalysis using data assimilation (Carton et al., 2000), and SeaWiFS-derived PP calculated following the VGPM model of Behrenfeld and Falkowski (1997). Temperature

¹ Chlorophyll and primary production data provided by the Ocean Productivity web site: <http://science.oregonstate.edu/ocean.productivity/>.

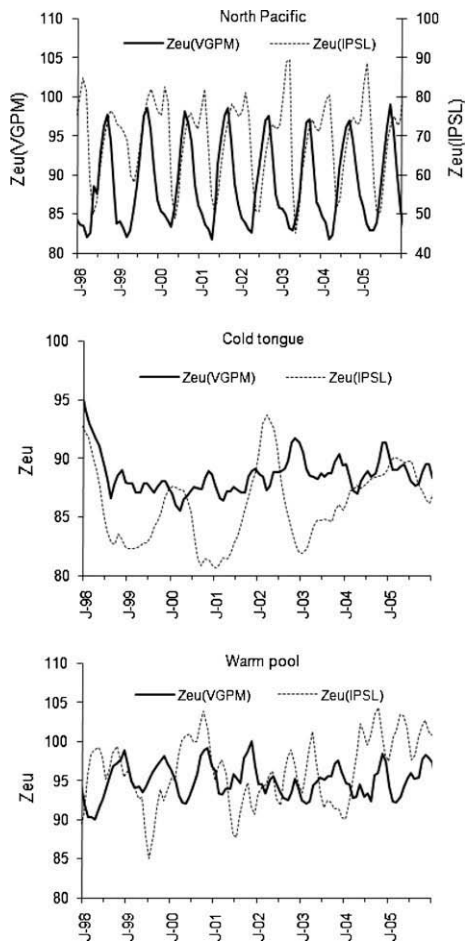


Fig. 1. Comparison of average euphotic depth, Z_{eu} (m), in three geographical regions: the North Pacific (40°N – 40°S ; 160°E – 150°W), the Cold Tongue (10°N – 10°S ; 180°W – 70°W) and the Warm Pool (10°N – 10°S ; 130°E – 165°E), between predictions from the IPSL Earth Climate simulation and the VGPM SeaWiFS-derived euphotic depth (Morel and Berthon, 1989; Behrenfeld and Falkowski, 1997).

differences between IPSL and SODA series do not exceed 1°C in the warm pool and cold tongue. Primary production is also in the same range in VGPM (SeaWiFS-derived) and IPSL series but higher in ESSIC series, roughly by a factor of two. The ESSIC simulation correctly predicted ENSO-related temperature and primary production variability in the tropical region. IPSL simulation also predicts an ENSO-type variability, with coherent changes between physics and biogeochemistry (Schneider et al., 2008). Though the climate model is not simulating ENSO events coinciding with real ones, the period used for the parameter estimation experiment (1985–2000) included an El Niño-like episode coinciding with the strong event observed in 1997–1998 (Figs. 2 and 3). This El Niño-like event is characterized by an expansion of warm waters in the eastern equatorial Pacific, a decrease in intensity of the equatorial upwelling, especially in the west, and a less oxygen-depleted upper layer in the east (Fig. 3).

At higher latitudes (North Pacific), the IPSL simulation better predicts the seasonal peaks than the ESSIC hindcast when compared to satellite-derived VGPM series (Fig. 2). The seasonal cycles of temperature of the three series (ESSIC, SODA and IPSL) are similar but present important discrepancies in the range of values: ESSIC being 4°C above the SODA series and IPSL 4°C below. The cold bias in the IPSL series is all the more surprising because the predicted euphotic depth used to average values in the epipelagic layer is shallower (~ 50 – 80 m) than the one based on satellite chlorophyll- a data to average the values of the SODA reanalysis. In-

deed, this cold bias occurs in middle and high latitudes in all basins and is a permanent feature of the IPSL (and some other) climate simulations. The bias is partly due to a shift of atmospheric structures (winds) towards the equator, and decreases when higher resolutions of the atmospheric model are tested. On the other hand, the warmer temperature predicted by the ESSIC simulation are likely due to the lack of a sea-ice model.

In summary, for the time period 1985–2000 that were used for parameter estimation, the ESSIC hindcast presents some biases in mid to high latitudes (seasonal signal and too warm temperatures at high latitudes), but works reasonably well in the tropics to simulate ENSO variability. However, this interannual signal is missing for oxygen concentration since we used climatology, and the vertical structure has been fixed and is constant over time in both east and west. The IPSL climate simulation has a good seasonal cycle at high latitudes, internally generated interannual variability close to observed ENSO variability in the tropics but not coinciding with observed events, a good coherence between changes in the vertical structure, primary production and dissolved oxygen concentration, but a strong cold temperature anomaly in the mid to high latitudes.

3.2. Optimization experiments

The parameter estimation of the SEAPODYM model for bigeye tuna was conducted using historical fishing data over the period 1985–2004 with the ESSIC hindcast and 1985–2000 with the IPSL climate simulation. Fishing data included spatially disaggregated monthly catch data for four purse-seine fisheries and two pole-and-line fisheries at an original resolution of $1^{\circ} \times 1^{\circ}$ and 15 long-line fisheries ($5^{\circ} \times 5^{\circ}$ resolution) with quarterly length frequency data associated with each fishery over the historical fishing period (data provided by the Secretariat of the Pacific Community and the Inter-American Tropical Tuna Commission). All together, these data represented 360,720 pairs of catch/effort observation and 1499 size-frequency distributions used in the parameter optimization. Fisheries from the Philippines–Indonesia region were included to account for total fishing mortality but were not used for optimization due to lack of spatial accuracy (Table 1).

Final estimates of the parameters in both experiments with ESSIC and IPSL data are presented in Table 2. The two experiments showed a generally good fit to these fishing data both for monthly catch time series and length–frequency distribution of catch (Fig. 4), and estimated parameter values were biologically plausible. The uncertainties of parameter estimates were provided by the diagonal elements of error-covariance matrix calculated as the inverse of the Hessian. For some parameters, particularly for the optimal temperatures T_0 and T_a (see Table 2), the uncertainties seem to be very small, hence the likelihood profiles for these parameters (within their boundaries) were computed and plotted to assure that its nearly quadratic shape permits local linearization.

Examples of spatial distribution of predicted biomass of young and adults are presented in Fig. 5 for two typical periods marked by El Niño and La Niña phases. As expected, results based on ESSIC hindcast forced by observed atmospheric fields (NCEP) were the most realistic, especially for the simulation of ENSO variability (Fig. 2). However, in this configuration, the biomass of adult bigeye tuna during the El Niño event in the eastern equatorial region was low while the catch was high. This is not the case in the experiment based on IPSL forcing that finally gives a better fit than the ESSIC-based experiment for longline fishing data in the equatorial region. This result can be attributed mostly to the use of climatology as a measure of oxygen in ESSIC experiment, which did not include prognostic oxygen in this version and does not represent the enhanced oxygen habitat in the eastern equatorial Pacific during an El Niño event, as in the IPSL experiment (Fig. 3). The second rea-

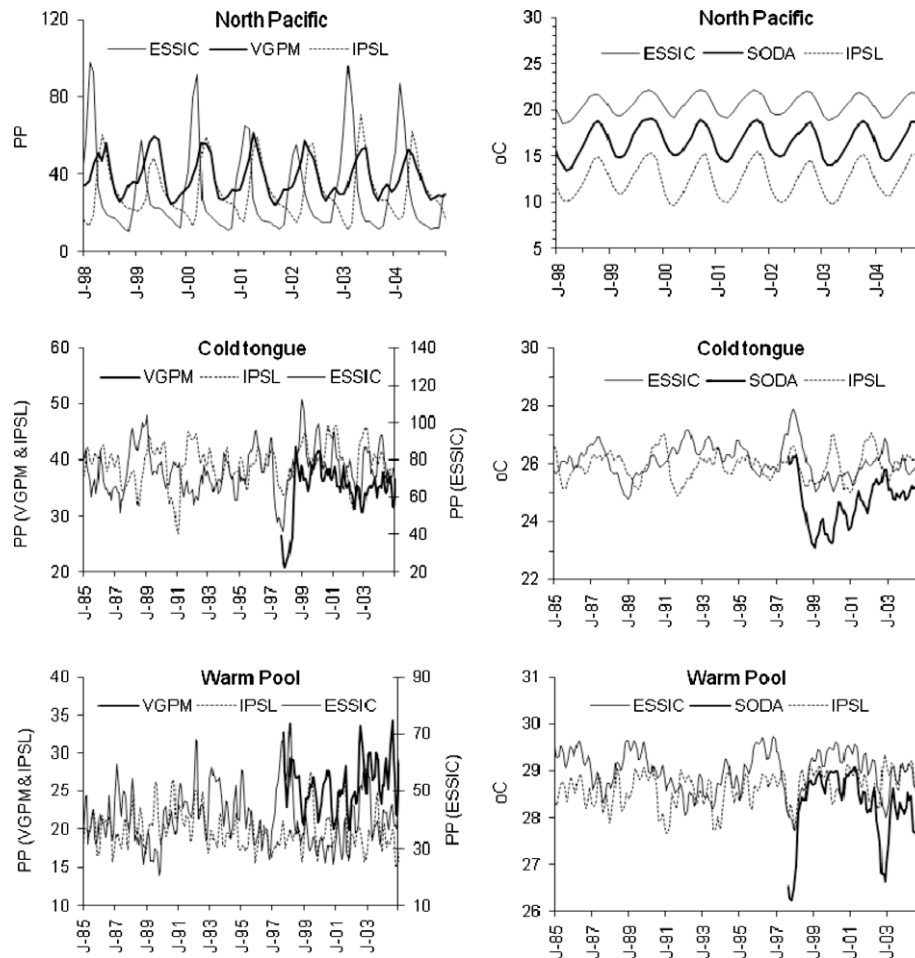


Fig. 2. Comparison of average vertically integrated primary production (left, in $\text{mmole C d}^{-1} \text{m}^{-2}$) and temperature (right, in $^{\circ}\text{C}$) in the epipelagic layer of three geographical regions: the North Pacific (40°N – 40°S ; 160°E – 150°W), the Cold Tongue (10°N – 10°S ; 180°W – 70°W) and the Warm Pool (10°N – 10°S ; 130°E – 165°E). The series are from ESSIC hindcast, IPSL Earth Climate simulation, the SODA reanalysis with data assimilation (Carton et al., 2000) and satellite-derived primary production calculated according to the VGPM model of Behrenfeld and Falkowski (1997). For temperature, the average in the epipelagic layer was based on the SeaWiFS-derived euphotic depth (Morel and Berthon, 1989; Behrenfeld and Falkowski, 1997) for SODA and IPSL, and the first 100 m for ESSIC.

son is the introduction of variable vertical boundary layers, related to the euphotic depth, in the version used with IPSL forcing. This change was introduced to have a better representation of the variability in vertical structure of the ocean. In particular, there is a well observed deepening of the thermocline in the east equatorial Pacific (cold tongue) during El Niño events, and conversely a shallowing in the west (warm pool), that can lead to substantial differences in mean fields of temperature, oxygen and currents by layer, as well as in the predicted prey (micronekton) distribution. At high latitudes, however, the ESSIC experiment provides the best fit to fishing data, mainly because the cold temperature bias of the IPSL-based experiment led to limited movement of adult fish and thus, lower biomass in these regions (Fig. 5).

Optimal spawning temperature was estimated to be 26.2°C with narrow standard deviation of the Gaussian function (0.8°C and 0.9°C) for both simulations. This range of temperature values corresponds typically to those observed at sea for mature and spawning bigeye tuna. For example, Schaefer et al. (2005) noted that in the eastern Pacific Ocean, bigeye tuna were spawning in water with sea surface temperature (SST) between 24°C and 30°C , with considerable numbers of mature females collected at SST between 24°C and 27°C , and the highest proportion of spawning at SST greater than 28°C . It should be noted here that temperature used in the model was an average of the epipelagic layer, thus lower than SST values. Optimal habitat temperature of the

oldest cohort was estimated to be 13°C with 2.16°C standard deviation using the ESSIC hindcast but a much lower value (8°C) with a large standard deviation (5°C) was estimated using the IPSL forcing fields. In fact, in the latter simulation both temperature parameters of adult's thermal habitat approached the imposed boundary values and hence were fixed in the final minimization experiment (and as such, it was impossible to compute SE for these parameters; see Table 2). This result was due to the strong cold temperature bias of the IPSL simulation in the temperate and subtropical regions where longline fleets catch a substantial amount of adult bigeye tuna. Despite a much lower optimal temperature over a larger distribution, the model had difficulties fitting these observations. The resulting thermal habitat by age, based on the ESSIC hindcast, is shown in Fig. 6. The parameter α that scales the contribution of the prey-predator larvae trade-off mechanism in the spawning index was lower for the IPSL-based experiment. It means that the higher contribution of temperature in defining the habitat gives a more diffuse and extended spawning area. In other words, the environmental forcing is not realistic enough to allow the model to predict more concentrated but highly favourable spawning zones combining abundance of prey and low biomass of predators for larvae. Since the spawning activity occurs in the warm waters of the tropical region, this result could be logically attributed to the less realistic prediction of the interannual (ENSO) variability in the climate simulation.

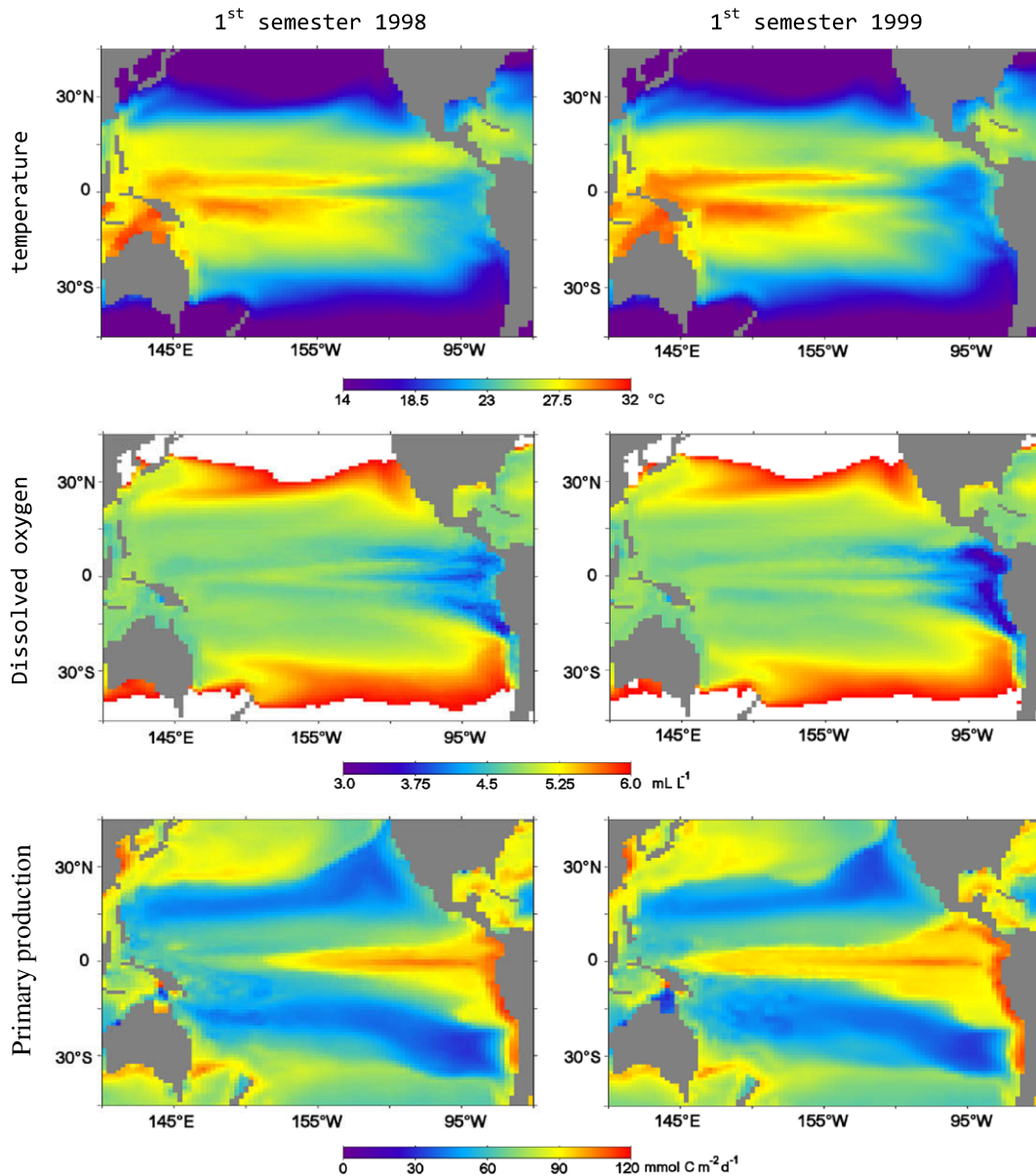


Fig. 3. El Niño-type event in IPSL Earth Climate model simulation. Left: 1st semester 1998 “El Niño”, and right: 1st semester 1999 “La Niña”. From top to bottom: temperature and dissolved oxygen concentration in the epipelagic layer, and vertically integrated primary production.

Physiological experiments suggest that bigeye tuna are more tolerant to low ambient oxygen than other tuna species (Brill, 1994; Lowe et al., 2000), with tolerance ranging between 0.5 and 1.0 mL O₂ L⁻¹ (Sharp, 1978; Sund et al., 1980). The estimated oxygen threshold parameter increased from 0.46 to 1.02 mL L⁻¹ between ESSIC- and IPSL-based experiments respectively (Table 2; Fig. 6). This change was associated with the use of climatological oxygen fields in the ESSIC experiment and with prognostic monthly oxygen fields in IPSL. The latter however, is coherent with seasonal and interannual variability of other environmental factors (especially temperature and primary production).

Natural mortality rates are the most difficult parameters to estimate in population dynamic models. For bigeye tuna, the mortality rate was estimated to be 0.03 month⁻¹ by analysis of catch-at-age data for the longline fishery, i.e., for large fish (Suda and Kume, 1967). Other estimates obtained from analyses of tagging data in the western Pacific Ocean range from 0.56 month⁻¹ for small fish (20–40 cm) to 0.04 month⁻¹ for 60–110 cm fish (Hampton et al.,

1998). In SEAPODYM, natural mortality is defined by the combination of two functions (Fig. 6) allowing mortality rates to vary with age (size) but also spatially and temporally within a range of values related to the habitat index. Parameters estimated for the functions in both experiments produced reasonable natural mortality coefficients-at-age comparable to other studies (Fig. 6) but with higher values for the oldest cohorts. The parameter β_3 that constrains this part of the curve however, is the most difficult to estimate by the model (Table 2).

The asymptote value of the Beverton–Holt relationship, R_5 is also difficult to estimate in population dynamics models. The SEAPODYM optimizer estimated R_5 with relatively large uncertainty. This parameter defines the number of larvae released in each cell of the grid in relation to spawning biomass and weighted by the spawning index (Fig. 6). This value, together with mortality rates, determines the total population size.

Estimated diffusion (D_{\max}) gives diffusion rates ranging on average from 560 nmi² day⁻¹ (1037 km² day⁻¹) for young cohorts

Table 1
Definition of fisheries for the Pacific bigeye tuna SEAPODYM parameters optimization experiments.

Fishery Number	Nationality	Gear	Sub-region	Code
1	Japan, Korea, Chinese Taipei	Longline	1	LL1
2	Japan, Korea, Chinese Taipei	Longline	2	LL2
3	United States (Hawaii)	Longline	2	LL3
4	All	Longline	3	LL4–5
5	Papua New Guinea	Longline	4	LL6
6	Japan, Korea, Chinese Taipei and China	Longline	4	LL7–8
7	United States (Hawaii)	Longline	4	LL9
8	All excl. Australia	Longline	5	LL10
9	Australia	Longline	5	LL11
10	Japan, Korea, Chinese Taipei	Longline	6	LL12
11	Pacific Island Countries/Territories	Longline	6	LL13
12	All excl. Chinese Taipei and China	Longline	7	LL21
13	Chinese Taipei and China	Longline	7	LL22
14	Japan, Korea, Chinese Taipei	Longline	8	LL23
15	Japan, Korea, Chinese Taipei	Longline	9	LL24
16	All	Purse seine, log/FAD sets	3	WPSASS
17	All	Purse seine, school sets	3	WPSUNA
18	All	Purse seine, log/FAD sets, nearshore and central area	8	EPSASS
19	All	Purse seine, school, dolphin sets, log/FAD sets, offshore area	8	EPSUNA
20	Japan	Pole-and-line	1,2	PLSUB
21	All	Pole-and-line	3,4	PLTRO
22	Philippines, Indonesia	Handline (large fish)	3	COMMHL
23	Philippines, Indonesia	Miscellaneous (small fish)	3	ARTSURF

Table 2
Estimated values of model parameters based on optimization with ESSIC hindcast and IPSL climate change simulation (relative uncertainty is calculated as the ratio between standard deviation and the parameter value). Bold values highlight where are the largest uncertainties.

θ	Description of parameter	ESSIC		IPSL		
		Parameter \pm SD	Relative uncertainty	Parameter \pm SD	Relative uncertainty	
T_0	Spawning	Optimal temperature for spawning ($^{\circ}\text{C}$)	26.2 ± 0.013	5×10^{-4}	26.2 ± 0.002	7×10^{-5}
σ_0		Standard deviation in spawning temperature Gaussian function	0.82 ± 0.012	0.015	0.9 ± 0.008	0.009
α		Half saturation constant for the food to predator ratio in the spawning index	0.63 ± 0.02	0.03	0.34 ± 0.01	0.03
R_s		Maximal number of larvae at large spawning biomass of adults	$0.0045 \pm 6 \times 10^{-4}$	0.130	$0.017 \pm 9 \times 10^{-4}$	0.053
T_a	Feeding	Optimal habitat temperature for largest bigeye tuna ($^{\circ}\text{C}$)	13 ± 0.004	3×10^{-4}	8	
σ_a	habitat	Standard deviation in adult habitat temperature Gaussian function	2.16 ± 0.003	0.002	5	
O		Threshold oxygen value for optimal habitat (ml/l)	0.46 ± 0.0006	0.001	1.02 ± 0.002	0.002
β_p	Natural	Slope coefficient in predation mortality	0.073 ± 0.0006	0.008	0.088 ± 0.001	0.012
M_{\max}	mortality	Maximal mortality rate due to predation (month^{-1})	0.25 ± 0.003	0.012	0.39 ± 0.006	0.015
β_s		Slope coefficient in senescence mortality	-0.097 ± 0.008	0.082	-0.067 ± 0.007	0.100
A		Threshold age of tuna senescence mortality (month)	80.6 ± 0.008	10^{-4}	87.55 ± 0.013	1.4×10^{-4}
D_{\max}	Movement	Diffusion parameter (0.22 gives maximal $8209 \text{ nmi}^2 \text{d}^{-1}$ ($15,203 \text{ km}^2 \text{d}^{-1}$) diffusion for largest tuna in zero habitat)	0.22 ± 0.002	0.01	0.1 ± 0.001	0.013
V_{\max}		Maximal velocity (body length)	0.32 ± 0.002	0.006	0.19 ± 0.004	0.019

to $2830 \text{ nmi}^2 \text{day}^{-1}$ ($5241 \text{ km}^2 \text{day}^{-1}$) for adult fish in ESSIC simulation, and from $240 \text{ nmi}^2 \text{day}^{-1}$ ($444 \text{ km}^2 \text{day}^{-1}$) to $1300 \text{ nmi}^2 \text{day}^{-1}$ ($2408 \text{ km}^2 \text{day}^{-1}$) for IPSL. Parameters of directed movement (along positive gradient of habitat index) were estimated to be lower in the IPSL-based experiment with maximal velocity of 0.32 and 0.19 body lengths s^{-1} , respectively (Table 2). It should be noted that final movement velocities are computed as the sum of directed (behavioural) and passive (currents) components.

3.3. Hindcast and forecast simulations

Using the optimal parameters estimated by the maximum-likelihood approach described above, we ran the model starting in 1960 with initial conditions generated by a spin-up simulation and excluding the first 5 years from our evaluation to reduce the effect of initial conditions. Fig. 7 compares the estimates of adult bigeye tuna biomass in the western-central (WCPO) and eastern (EPO) Pacific Ocean for both the optimization period and hindcast

period with independent series from stock-assessment studies using the model MULTIFAN-CL (Hampton and Fournier, 2001; Hampton et al., 2006; Sibert et al., 2006). SEAPODYM estimates from the two experiments were very similar in the WCPO but the IPSL-based series predicts a constant higher biomass in the EPO that, as discussed above, is likely due to both a better definition of vertical structure and more coherent variability in simulated dissolved oxygen concentration. Despite the large uncertainty on the R_s parameter (see Section 3.2.), the final biomass predicted by SEAPODYM is of the same order as that obtained by an independent stock-assessment model, MULTIFAN-CL (Fig. 7). The latter, however, showed a higher variability and a stronger decreasing slope in the initial period of the industrial fishery (1965–1975). It is also worth noting that catch predictions in simulations based on ESSIC and IPSL forcing maintain a good fit outside of the time window used for optimization (Fig. 4).

The projection of the IPSL climate simulation under the A2 scenario for the 21st century results in a general increase of temperature. The average temperature of the first 100 m in the western

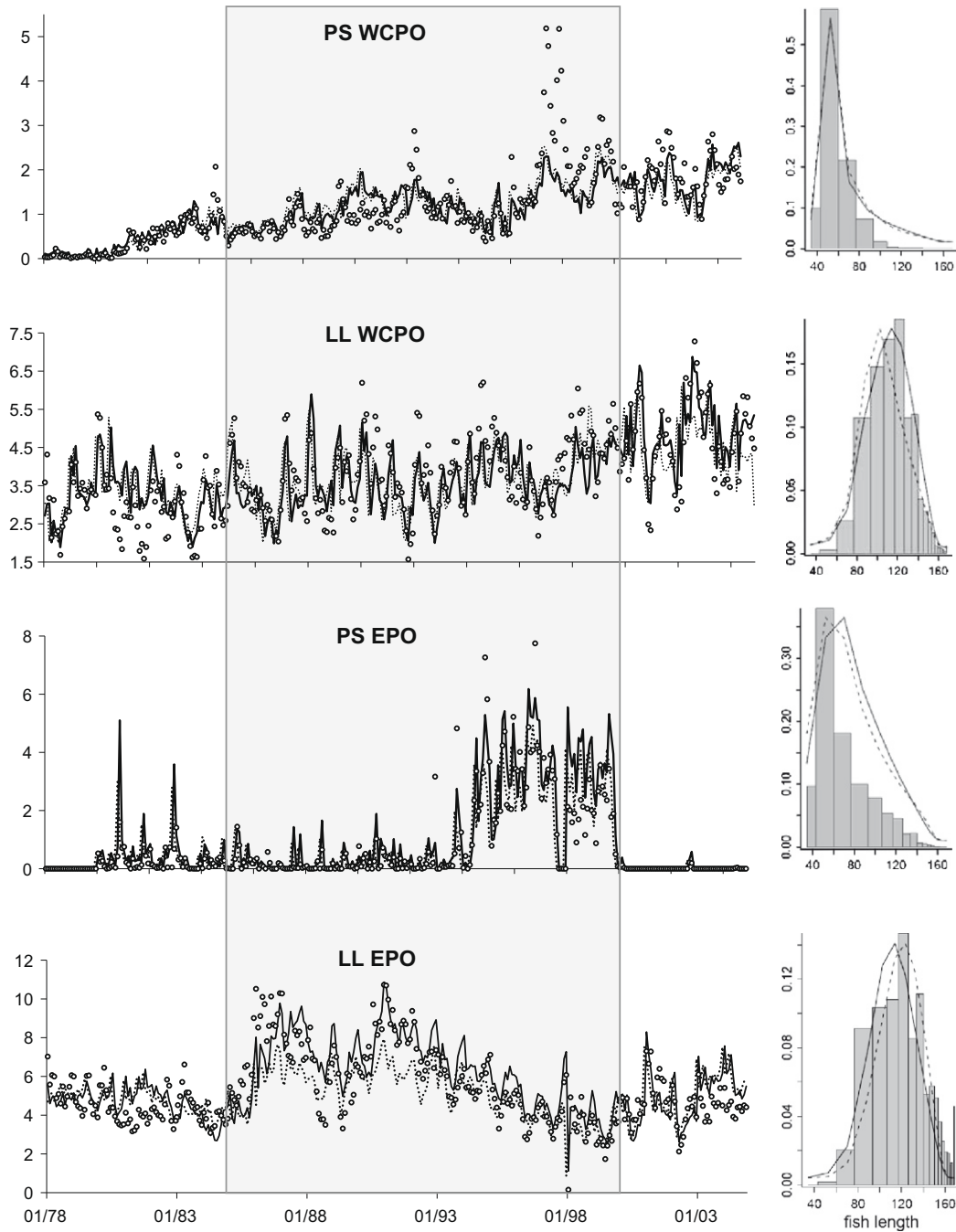


Fig. 4. Comparison of observed (circles) and predicted (lines) monthly catch series (in thousand metric tonnes) within (grey area) and outside of the optimization period and size-frequency distributions aggregated by main categories of fleets (PS = purse seine, LL = longline) in the western central (WCPO) and eastern Pacific Ocean (EPO); results from the IPSL-forced (black line) and ESSIC-forced (dotted line) experiments.

central Pacific region 10°N–10°S is just below 29 °C before 2000 and reaches 31 °C at the end of the century (Fig. 8). In the east, the increase leads to an average temperature of 26 °C, which is the predicted optimal spawning temperature for bigeye tuna. Primary production is projected to decrease in the tropics (Fig. 8) while euphotic depth increases in parallel. The decline of productivity in the tropical region is compensated by an increase in higher latitudes (not shown) where a higher vertical stability increases the length of the growing season for phytoplankton in the euphotic depth. The decrease in primary productivity predicted over the 21st century is particularly strong in the western tropical Pacific. Logically, the productivity of mid-trophic components follows sim-

ilar general trends (Fig. 8). The dissolved oxygen concentration, a critical variable constraining tuna habitat, is also predicted to decrease almost everywhere under this A2 scenario, with the exception of the sub-surface eastern tropical Pacific where dissolved O₂ is predicted to increase on average in the second half of the century (Fig. 8), leading to a mean state similar to that predicted under El Niño-like events (Fig. 3). Dissolved oxygen is controlled by temperature and salinity that determine oxygen solubility, by horizontal and vertical circulation controlling ocean ventilation, and by biological processes that produce oxygen in the euphotic layer through photosynthesis or consume it by respiration of organic matter in the mesopelagic layer. The primary reason for the simu-

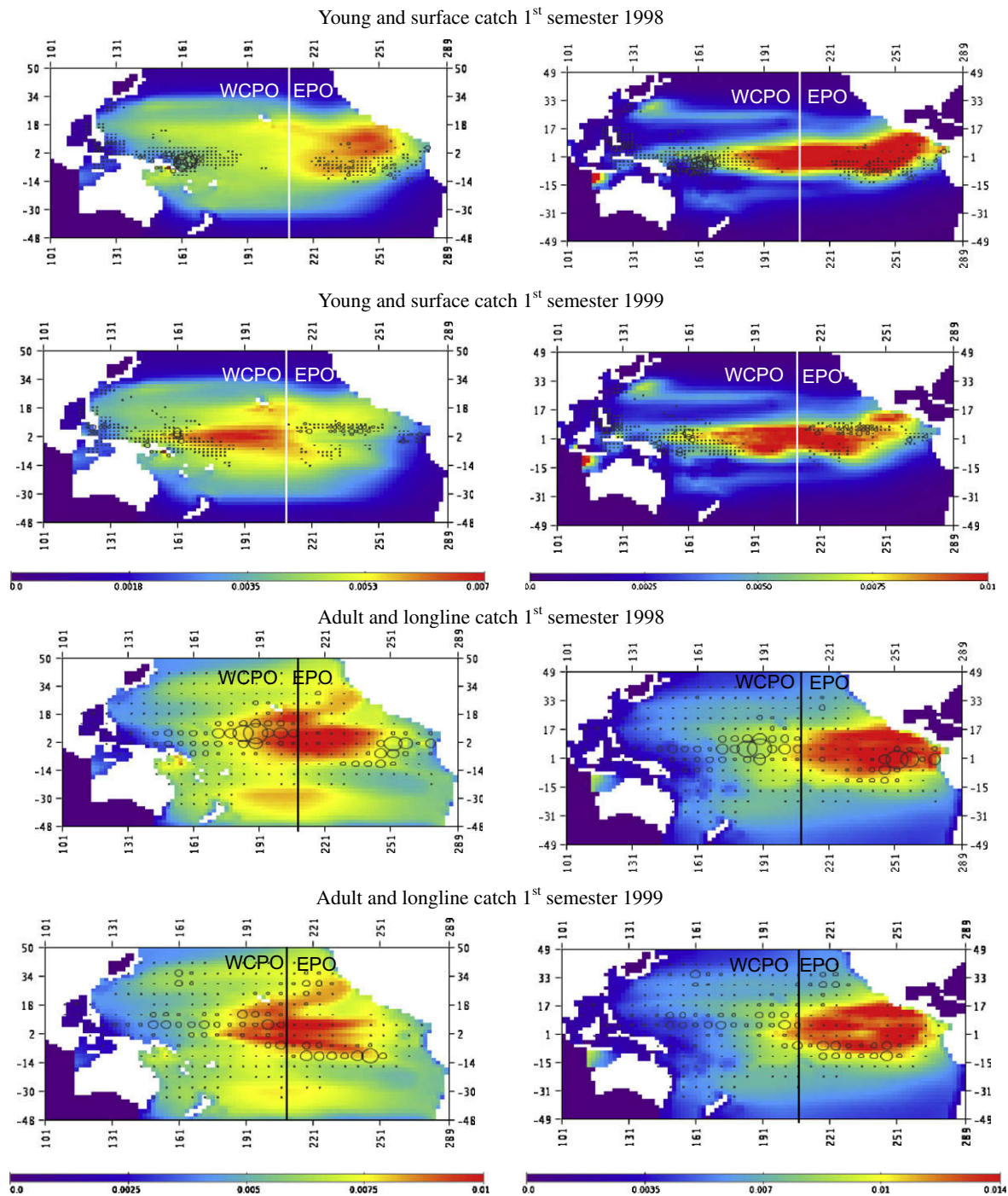


Fig. 5. Total catch (proportional to circles) observed in surface and longline fisheries superimposed on predicted young and adult bigeye tuna biomass (g m^{-2}) distribution respectively, for the 1st semester 1998 (El Niño phase) and 1st semester 1999 (La Niña phase). Results of both optimization experiments using ESSIC (left) and IPSL (right) forcing fields are compared.

lated decrease in oxygen is thought to be the reduction of transport to depth due to increased vertical stability and solubility changes due to warmer waters (Matear et al., 2000; Bopp et al., 2002; Plattner et al., 2002). The increase in the sub-surface eastern equatorial Pacific Ocean is likely to be a combination of biological changes (decreasing primary productivity) and physical changes (Gnanadesikan et al., 2007).

The parameterization derived for the IPSL simulation over the period 1985–2000 was used for the entire period of the simulation (1860–2100), without fishing effort, to investigate general trends and the spatial distribution of biomass associated with environ-

mental changes under increasing forcing of atmospheric CO_2 . The result is a clear expansion of the spawning habitat and density of larvae (Fig. 9) from the tropics towards higher latitudes, correlated with the temperature increase. Since production at low and mid-trophic levels decreases in parallel, there is likely only limited change to the spawning habitat ratio that represents the trade-off between presence of food and absence of predators of larvae.

The eastern tropical Pacific also becomes much more favourable for bigeye tuna spawning (Fig. 9) with a pronounced increase of larval biomass during the century (Fig. 8). In this region, while the surface temperature becomes optimal for bigeye tuna spawning, the

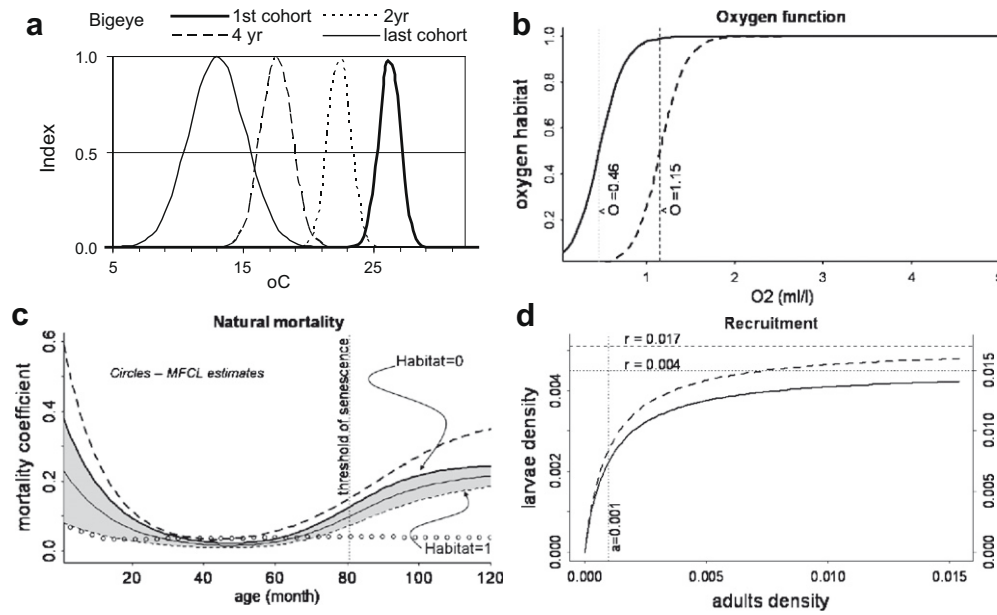


Fig. 6. Representation of the main habitats and population dynamic characteristics of Pacific bigeye tuna obtained through parameter optimization process based on the ESSIC forcing data set and fishing data for 1985–2004. (a) Change in habitat temperature by cohort; (b) oxygen function; (c) mortality coefficient-at-age (month⁻¹) with range of variability linked to habitat values and estimates from MULTIFAN-CL (circles); (d) Beverton–Holt relationship (at the grid cell level). Changes with simulation using IPSL–PISCES climate forcing fields is shown with dotted line in (b, c, and d).

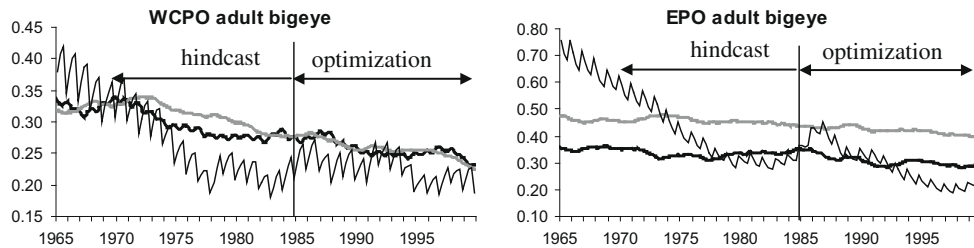


Fig. 7. Biomass trends (million tonnes) in Pacific bigeye tuna population predicted in WCPO and EPO with optimization (1985–2004) and hindcast prediction to 1965 for the two experiments based on ESSIC (black thick line) and IPSL (grey line) forcing fields. The trends for adults are compared to estimates (thin black line) from stock-assessment model MULTIFAN-CL (Hampton et al., 2006; Sibert et al., 2006).

adult habitat also improves due to the increase in dissolved oxygen concentration allowing adults to access deeper forage. Because there is a better habitat, the biomass of mature adults increases and has a positive feedback on the local mechanism of stock recruitment following the Beverton–Holt relationship.

In the Western Central Pacific, the situation is quite different. The temperature becomes too warm in the equatorial region for bigeye tuna spawning and if the total biomass of larvae still slowly increases (Fig. 8), it is due to the increasing contribution of sub-tropical areas to the spawning habitat (Fig. 9). Despite this slight increase in larval density, the ensuing adult biomass remains stable and even declines at the end of the century (Fig. 8). The differential between these two trends can be explained by the increasing mortality of older stages due to lower habitat values (too warm temperatures in surface waters, decreasing oxygen concentration in sub-surface waters, and less food), and to the displacement of surviving fish to the eastern region.

4. Discussion

This study demonstrates that our model SEAPODYM can offer a new component to be coupled to climate models and used to investigate the potential impact of global warming on the upper levels of the ocean ecosystem, to explore how the numerous and

complex physical and biogeochemical predicted changes can interact with population dynamics of oceanic top predators.

The optimization approach and the evaluation based on historical fishing data are key steps to give confidence to the model estimates. Optimization experiments provided reasonable values of the biological parameters with narrow standard deviation and fully consistent with existing knowledge. Despite the large uncertainty in the R_s parameter, the level of biomass estimated with the two optimization experiments are finally close to that obtained through an independent approach with the stock-assessment model MULTIFAN-CL used by the Western Central Pacific Tuna Commission. The biomass trend estimated by this latter model diverged from the SEAPODYM hindcast estimates in the beginning of the series, during the 1960s. There are potentially many reasons for this divergence that we will continue to investigate, e.g. the sensitivity to initial conditions, the underestimation of oceanic variability by the models; or for the stock-assessment model, too few data at the beginning of the fisheries to constrain the model. Nevertheless, the capacity of the model to predict plausible responses at a basin-scale level is an essential development given the significance of bigeye tuna both as an exploited species and as a top predator in the pelagic ecosystem. The good fits between predicted and observed catch and size frequencies fishing data, within and, notably, outside the optimization time window increased the

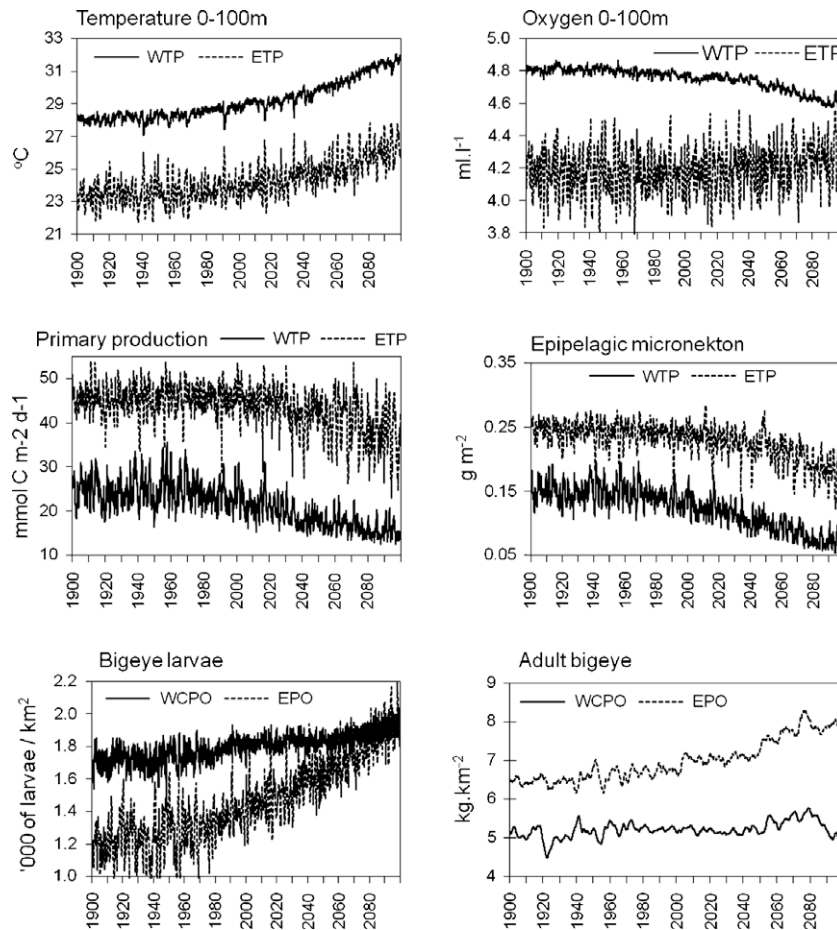


Fig. 8. Trends (1900–2100) for temperature and dissolved oxygen in the epipelagic layer, vertically integrated primary production predicted by the IPSL–PISCES climate simulation in the western (WTP: 20°N–20°S; 130°E–150°W) and eastern (ETP: 20°N–20°S; 150°W–80°W) tropical Pacific under the IPCC A2 scenario, and resulting SEAPODYM predictions of epipelagic micronekton biomass, larvae and adult bigeye tuna in the western central (WCPO) and Eastern (EPO) Pacific Ocean.

confidence in the model and simulation results, especially considering the small number of parameters used in the model to describe the spatial population dynamics at basin scale and for a fully closed life cycle.

Due to important discrepancies between oceanic environments from the hindcast and the Climate Earth experiments, it was necessary to re-estimate parameter values obtained during optimization experiments with the ESSIC hindcast to account for the new “IPSL environment”, especially since there were different vertical layer definitions, different biases in temperature, and prognostic versus climatological data for dissolved oxygen concentration. Thus, we conducted a second series of optimization experiments using IPSL climate model forcing and historical fishing data. The natural variability in the bigeye tuna population can be explained roughly by the sum of a mean state with seasonal and interannual signals. Bigeye tuna have an extended habitat in regards to temperate latitudes, at least for adults (Fig. 5), and hence under the seasonal influence, that is well simulated by the IPSL model. The interannual (ENSO) variability is the strongest in the tropical region and particularly in the upper layer where large changes in currents, temperature, primary production, and consequently epipelagic forage, control the larvae and juvenile habitats and dynamics. But ENSO variability has less impact on adult fish that can access deeper and more stable (meso- and bathypelagic) forage biomass, or move seasonally to temperate latitudes. Therefore, it was not surprising that optimization experiments with IPSL climate simulation environment and historical fishing data, dominated by longline catch of adult bigeye tuna, were able to capture

the main signals of population dynamics despite an interannual signal not in phase with the observed one. In addition, in the time period used for optimization (1985–2000) the IPSL simulation predicted (by chance) an El Niño-type event coinciding with the strong event of 1997–1998.

Observed changes in parameter values between the two optimization experiments using ESSIC and IPSL forcing fields were consistent and highlighted the sensitivity of the population dynamics to the predicted oceanic environment. For example, the increase in estimated values for the oxygen threshold parameter between optimization experiments forced by ESSIC and IPSL is linked in the latter experiment to the use of both a shallower vertical structure in the eastern tropical Pacific and predicted interannual variability in oxygen concentration showing an increase in the same region during El Niño-type events. Obviously, this increase of oxygen concentration does not appear in the monthly climatology.

A bias or anomaly in the oceanic environment is also quickly detected through the optimization approach because the model can not converge in estimating plausible parameters values. This was the case for the optimization of adult thermal habitat, clearly because the IPSL experiment had a cold temperature anomaly in high latitudes. Conversely, temperature was not biased in the tropical region and the model successfully estimated a plausible optimal temperature for spawning very close to the one obtained with ESSIC hindcast.

A cold temperature anomaly in IPSL simulation is a major issue given the key effects of temperature on the dynamics of both mid-trophic components and tuna populations. It is essential to reduce

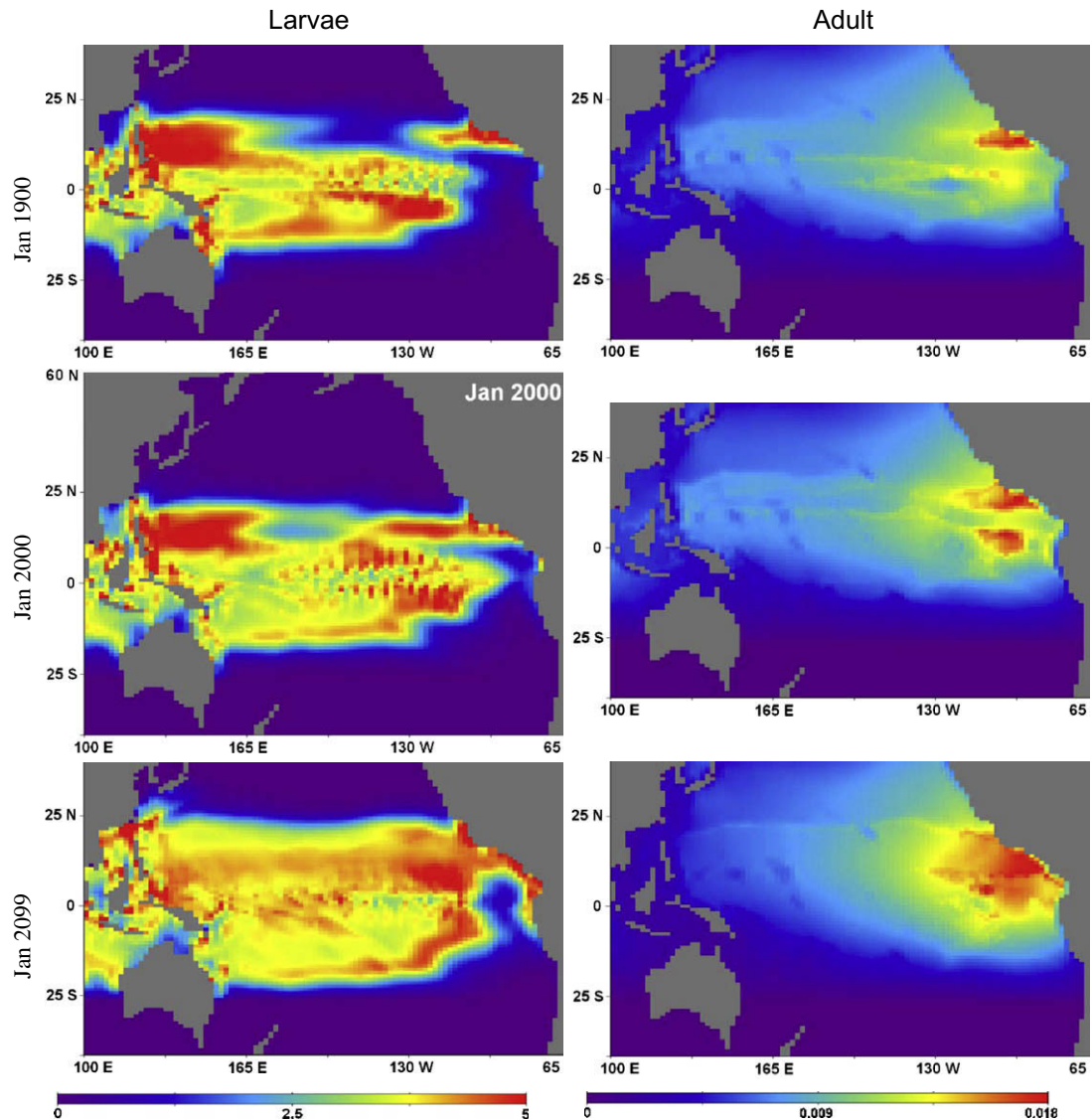


Fig. 9. Density distribution of Pacific bigeye tuna larvae (left, in number km^{-2}) and adult biomass (right, in t km^{-2}) predicted with SEAPODYM in January of year 1900, 2000 and 2099 (from top to bottom) using forcing fields from the IPSL-PISCES climate simulation (IPCC SRES-A2 scenario).

this bias to improve further analyses of climate change impacts on tuna. The cause of this bias has been identified and is partly due to a too coarse spatial resolution of the atmospheric model, leading to a shift of the storm tracks towards the Equator. Simulation tests have effectively shown that the bias is reduced with increasing resolution. This would mean however, that this cold anomaly is also associated with other biases (currents, primary production, oxygen, etc.). Therefore, since storage and computing capacity are limiting factors when running Earth Climate models that are coupling many components of the system, a solution could be to consider simulations over several shorter periods (e.g., 20–30 years) with higher resolution, and at regular intervals in historical and projected time series. More generally, a high resolution experiment limited to a projection for the coming two or three decades and with a realistic interannual variability in the historical period, would be of major interest for investigating climate change impacts on marine species.

Results from this study also highlight the intricacy of the impacts of global climate change on marine pelagic populations. The model prediction suggests complex patterns, with different mechanisms (i.e. advection, natural mortality, stock–recruitment

relationship) that can lead to multiple nonlinear processes and different responses of adult populations. While the projected climate change impact leads to expansion of favourable spawning habitat toward subtemperate latitudes, an effect that can be expected given the temperature increase and the tropical affinities of the species, it is the eastern tropical Pacific that becomes more favourable for bigeye tuna spawning. However, latitudinal expansion in this simulation experiment is limited by the cold anomaly, and could be even more important without this bias. In the western Pacific, the warm pool becomes really too warm for favourable bigeye tuna spawning (optimal temperature is 26.2°C), but increasing contribution of subtropical areas to the spawning habitat results in a slight increasing trend in total larvae biomass. Without considering fishing impact, the adult biomass in this Pacific region remains stable and starts to decrease at the end of the century, likely by the increasing mortality associated with lower habitat values and with displacement of surviving fish to the eastern and temperate region. The declining habitat is a result of the combination of too warm temperatures near the surface, decreasing oxygen concentration in sub-surface waters, and a decrease of prey biomass that were

already at relatively low levels in this region. In the eastern Pacific, the situation is becoming more favourable both for spawning and for feeding habitat. Even if prey biomass decreases there is still high productivity, and deep forage becomes more accessible due to increased oxygen concentration.

Recent observations have shown evidence for a decrease in oxygen concentrations, which is likely driven by reduced rates of water renewal in the thermocline (100–1000 m) in most ocean basins from the early 1970s to the late 1990s (IPCC, 2007). This decrease is attributed to seawater warming and to reduced ventilation of water masses in the ocean. An increase in the carbon-to-nitrogen ratio of organic matter formed at higher CO₂ levels and to the respiration of this excess organic carbon could also contribute to this reduction (Oschlies et al., 2008). Consistent with these recent observations, the IPSL A2 simulation showed decreased oxygen concentrations in the thermocline at mid and high latitudes, particularly in the North Pacific between 40°N and 60°N, driven by increased vertical stratification and reduced rates of water formation. However, the significant increase of oxygen concentration in the eastern equatorial ocean predicted by the IPSL simulation would need to be confirmed by long-term observations and other models results. Given the critical impact that dissolved oxygen concentration can have on the habitat and thus distribution of bigeye tuna and other fish species in the eastern Pacific, a particular focus should be given to this issue and dissolved oxygen concentration should be carefully monitored in this region.

Finally, applications of SEAPODYM to other tuna species with different biological characteristics (e.g. skipjack and yellowfin tunas) and analyses of predictions obtained in other oceans should provide further independent evaluations of the model. SEAPODYM has the potential to be a powerful tool for evaluating the relative impacts of different human activities on populations of large predatory fish. Once plausible forcing fields are established, it is a relatively straightforward task to estimate the relative impacts of fishing and climate change on tuna populations over the last half century because measures of fishing effort are already available. However, projection of fishing impact to the end of the century will require some means to project fishing mortality into the future.

Acknowledgments

We would like to acknowledge Peter Williams (SPC) and Michael Hinton (IATTC) for preparing and supplying catch and size composition data. We also thank the Ocean Productivity team for providing us the SeaWiFS-derived primary production. This work was funded by the Marine Ecosystems Modeling and Monitoring by Satellite section in CLS, France, the Cooperative Agreement NA17RJ1230 between the Joint Institute for Marine and Atmospheric Research (JIMAR) and the National Oceanic and Atmospheric Administration (NOAA), and by the European-funded Pacific Regional SciFish Programme of the Oceanic Fisheries Programme of the Secretariat of the Pacific Community. Views expressed in the paper do not necessarily represent the views of these agencies or organizations. Murtugudde gratefully acknowledges NASA and NOAA Carbon and Mesoscale grants that supported part of his involvement.

Appendix A

For parameter estimation, the catch and size data were used to construct the cost function. The predicted catch $C_{t,f,i}^{pred}$ is computed in the model as follows:

$$C_{t,f,i}^{pred} = q_f E_{t,f,i} \sum_{a=1}^K s_{fa} \omega_a N_{t,f,i} \Delta x \Delta y,$$

where indices t, f, i, j denote time, fishery and space correspondingly, q_f – catchability coefficient intrinsic to each fishery, $E_{t,f,i}$ – spatially distributed fishing effort at monthly time step t for all fisheries f , s_{fa} – selectivity coefficients computed as functions of length at age a (two types of functions we used – sigmoid and non-symmetric Gaussian), ω_a – average weight in a th cohort, $N_{t,f,i}$ – population density that is computed for each cohort and spatial position of the domain.

To utilize size data we constructed relative variables:

$$Q_{t,far}^{pred} = \frac{s_{fa} \sum_{i,j \in r} E_{t,f,i} N_{t,f,i} \Delta x \Delta y}{\sum_{a=1}^K s_{fa} \sum_{i,j \in r} E_{t,f,i} N_{t,f,i} \Delta x \Delta y},$$

where r is the index for region for which the size data were sampled. Note that depending on data availability we used different time stratification for catch and size data, i.e., catch terms contributed to the likelihood every month while length frequencies terms were aggregated over quarter.

Hence, the cost function, which is specified as the sum of log-negative Poisson likelihood for catch data and normal likelihood component for size data is computed as

$$J = -\ln L(\theta | C^{obs}, Q^{obs}) \\ = \sum_{t,f,i} (C_{t,f,i}^{pred} - C_{t,f,i}^{obs} \ln C_{t,f,i}^{pred} + \ln \Gamma(C_{t,f,i}^{obs})) + \frac{1}{2\sigma_Q^2} \sum_{t,far} (Q_{t,far}^{pred} - Q_{t,far}^{obs})^2$$

and minimized using quasi-Newton method.

References

- Aumont, O., Orr, J.C., Monfray, P., Madec, G., Maier-Reimer, E., 1999. Nutrient trapping in the equatorial Pacific: the ocean circulation solution. *Global Biogeochemical Cycles* 13, 351–369.
- Aumont, O., Bopp, L., 2006. Globalizing results from ocean in situ iron fertilization studies. *Global Biogeochemical Cycles* 20, GB2017. doi:10.1029/2005GB002591.
- Bard, Y., 1974. Nonlinear Parameter Estimation. Academic Press, New York, USA.
- Behrenfeld, M.J., O'Malley, R.T., Siegel, D.A., McClain, C.R., Sarmiento, J.L., Feldman, G.C., Milligan, A.J., Falkowski, P.G., Letelier, R.M., Boss, E.S., 2006. Climate-driven trends in contemporary ocean productivity. *Nature* 444, 752–755.
- Behrenfeld, M.J., Falkowski, P.G., 1997. A consumer's guide to phytoplankton primary productivity models. *Limnology and Oceanography* 42, 1479–1491.
- Bopp, L., LeQuéré, C., Heimann, M., Manning, A.C., Monfray, P., 2002. Climate-induced oceanic oxygen fluxes: implications for the contemporary carbon budget. *Global Biogeochemical Cycles*, 16. doi:10.10292001GB001445.
- Bopp, L., Monfray, P., Aumont, O., Dufresne, J.L., Le Treut, H., Madec, G., Terray, L., Orr, J.C., 2001. Potential impact of climate change on marine export production. *Global Biogeochemical Cycles* 15, 81–99.
- Bopp, L., Aumont, O., Cadule, P., Alvain, S., Gehlen, M., 2005. Response of diatoms distribution to global warming and potential implications: a global model study. *Geophysical Research Letters* 32 (19), L19606, doi:10.1029/2005GL019606.
- Boyd, P.W., Doney, S.C., 2002. Modeling regional responses by marine pelagic ecosystems to global climate change. *Geophysical Research Letter* 29 (16), 1806. doi:10.1029/2001GL014130.
- Brill, R.W., 1994. A review of temperature and oxygen tolerance studies of tunas pertinent to fisheries oceanography, movement models and stock assessments. *Fisheries Oceanography* 3, 204–216.
- Carton, J.A., Chepurin, G., Cao, X., Giese, B.S., 2000. A simple ocean data assimilation analysis of the global upper ocean 1950–1995. Part 1: methodology. *Journal of Physical Oceanography* 30, 294–309.
- Christian, J.R., Verschell, M.A., Murtugudde, R., Busalacchi, A.J., McClain, C.R., 2002. Biogeochemical modelling of the tropical Pacific Ocean: I. Seasonal and interannual variability. *Deep Sea Research, Part II* 49, 509–543.
- Cox, P.M., Betts, R.A., Jones, C.D., Spall, S.A., Totterdell, I.J., 2000. Acceleration of global warming due to carbon cycle feedbacks in a 3D coupled model. *Nature* 408, 184–187.
- Cubasch, U., Meehl, G.A., Boer, G.J., Stouffer, R.J., Dix, M., Noda, A., Senior, C.A., Raper, S., Yap, K.S., 2001. Projections of future climate change. In: Houghton, J.T., Ding, Y., Griggs, D.J., Noguer, M., van der Linden, P.J., Dai, X., Maskell, K., Johnson, C.A. (Eds.), *Climate change 2001: The Scientific Basis*. Cambridge University Press, New York, pp. 525–582.
- Denman, K., Hofmann, E., Marchant, H., 1996. Marine biotic responses to environmental change and feedbacks to climate. In: Houghton, J.T., Meira Filho, L.G., Callander, B., Maskell, K. (Eds.), *Climate Change 1995: The Scientific Basis*. Cambridge University Press, New York, pp. 483–516.
- Fasham, M.J.R., Ducklow, H.W., McKelvie, S.M., 1990. A nitrogen based model of plankton dynamics in the oceanic mixed layer. *Journal of Marine Research* 48, 591–639.

- Garcia, H.E., Locarnini, R.A., Boyer, T.P., Antonov, J.I., 2006. World Ocean Atlas 2005, volume 3: dissolved oxygen, apparent oxygen utilization, and oxygen saturation. In: Levitus, S. (Ed.), NOAA Atlas NESDIS 63 US. Government Printing Office, Washington, DC, p. 42.
- Gnanadesikan, A., Russell, J.L., Zeng, F., 2007. How does ocean ventilation change under global warming? *Ocean Science* 3, 43–53.
- Hampton, J., Bigelow, K., Labelle, M., 1998. A summary of current information on the biology, fisheries and stock assessment of bigeye tuna (*Thunnus obesus*) in the Pacific Ocean, with recommendations for data requirements and future research. Secretariat of the Pacific Community, Noumea, New Caledonia, Oceanic Fisheries Programme. Technical Report No. 36, 59 pp. ISBN: 982-203-628-4.
- Hampton, J., Fournier, D., 2001. A spatially disaggregated, length-based, age-structured population model of yellowfin tuna (*Thunnus albacares*) in the western and central Pacific Ocean. *Marine Freshwater Research* 52, 937–963.
- Hampton, J., Langley, A., Kleiber, P., 2006. Stock assessment of bigeye tuna in the western and central Pacific Ocean, including an analysis of management options. In: 2nd Meeting of the Scientific Committee of the Western and Central Pacific Fisheries Commission, Manila, Philippines, 7–18 August, 2006, 103 pp (WCPFC-SC2-SA WP-2).
- IPCC, 2007. Climate Change 2007: Synthesis report. contribution of working groups I, II and III to the fourth assessment. In: Core Writing Team, Pachauri, R.K., Reisinger, A. (Eds.), Report of the Intergovernmental Panel on Climate Change. IPCC, Geneva, Switzerland, 104 pp.
- Lehodey, P., Chai, F., Hampton, J., 2003. Modelling climate-related variability of tuna populations from a coupled ocean-biogeochemical-populations dynamics model. *Fisheries Oceanography* 12, 483–494.
- Lehodey, P., Murtugudde, R., Senina, I., 2010. Bridging the gap from ocean models to population dynamics of large marine predators: a model of mid-trophic functional groups. *Progress in Oceanography*. doi:10.1016/j.pocean.2009.09.008.
- Lehodey, P., Senina, I., Murtugudde, R., 2008. A spatial ecosystem and populations dynamics model (SEAPODYM) – modelling of tuna and tuna-like populations. *Progress in Oceanography* 78, 304–318.
- Lowe, T.E., Brill, R.W., Cousins, K.L., 2000. Blood oxygen-binding characteristics of bigeye tuna (*Thunnus obesus*), a high-energy-demand teleost that is tolerant of low ambient oxygen. *Marine Biology* 136, 1087–1098.
- Marti, O., Braconnot, P., Bellier, J., Benshila, R., Bony, S., Brockmann, P., Cadule, P., Caubel, A., Denvil, S., Dufresne, J.-L., Fairhead, L., Filiberti, M.-A., Foujols, M.-A., Fichet, T., Friedlingstein, P., Gosse, H., Grandpeix, J.-Y., Hourdin, F., Krinner, G., Lévy, C., Madec, G., Musat, I., de Noblet, N., Polcher, J., Talandier, C., 2006. The New IPSL Climate System Model: IPSL-CM4, Note du Pôle de Modélisation no. 26. ISSN:1288-1619.
- Matear, R.J., Hirst, A.C., McNeil, B.I., 2000. Changes in dissolved oxygen in the Southern Ocean with climate change. *Geochemistry, Geophysics, and Geosystems* 1, 1050. doi:10.1029/2000GC000086.
- Morel, A., Berthon, J.-F., 1989. Surface pigments, algal biomass profiles, and potential production of the euphotic layer: relationships reinvestigated in view of remote-sensing applications. *Limnology Oceanography* 34, 1545–1562.
- Oschlies, A., Schulz, K.G., Riebesell, U., Schmittner, A., 2008. Simulated 21st century's increase in oceanic suboxia by CO₂-enhanced biotic carbon export. *Global Biogeochemical Cycles* 22, GB4008. doi:10.1029/2007GB003147.
- Plattner, G.K., Joos, F., Stocker, T.F., 2002. Revision of the global carbon budget due to changing air–sea oxygen fluxes. *Global Biogeochemical Cycles* 16, 1096. doi:10.10292001GB001746.
- Sarmiento, J.L., Slater, R.D., Fasham, M.J.R., Ducklow, H.W., Toggweiler, J.R., Evans, G.T., 1993. A seasonal three-dimensional ecosystem model of nitrogen cycling in the North Atlantic euphotic zone. *Global Biogeochemical Cycles* 7, 417–450.
- Sarmiento, J.L., Slater, R., Barber, R., Bopp, L., Doney, S.C., Hirst, A.C., Kleypas, J., Matear, R., Mikolajewicz, U., Monfray, P., Soldatov, V., Spall, S.A., Stouffer, R., 2004. Response of ocean ecosystems to climate warming. *Global Biogeochemical Cycles* 18, 23.
- Schaefer, K.M., Fuller, D.W., Miyabe, N., 2005. Reproductive biology of bigeye tuna (*Thunnus obesus*) in the Eastern and Central Pacific Ocean. *Inter-American Tropical Tuna Commission Bulletin* 23, 1–31.
- Schneider, B., Bopp, L., Gehlen, M., Segsneider, J., Frölicher, T.L., Cadule, P., Friedlingstein, P., Doney, S.C., Behrenfeld, M.J., Joos, F., 2008. Climate-induced interannual variability of marine primary and export production in three global coupled climate carbon cycle models. *Biogeosciences* 5, 597–614.
- Senina, I., Sibert, J., Lehodey, P., 2008. Parameter estimation for basin-scale ecosystem-linked population models of large pelagic predators: application to skipjack tuna. *Progress in Oceanography* 78, 319–335.
- Sharp, G.D., 1978. Behavioral and physiological properties of tuna and their effects on vulnerability to fishing gear. In: Sharp, G.D., Dizon, A.E. (Eds.), *The Physiological Ecology of Tunas*. Academic Press, New York.
- Sibert, J., Hampton, J., Kleiber, P., Maunder, M., 2006. Biomass, size, and trophic status of top predators in the Pacific Ocean. *Science* 314, 1773–1776.
- Suda, A., Kume, S., 1967. Survival and recruitment of bigeye tuna in the Pacific Ocean, estimated by the data of tuna longline catch. *Nankai Regional Fisheries Research Laboratory Report* 25, 91–104.
- Sund, P.N., Blackburn, M., Williams, F., 1980. Tunas and their environment in the Pacific Ocean: a review. *Oceanography Marine Biology Annual Review* 19, 443–512.
- Wang, X., Christian, J.R., Murtugudde, R., Busalacchi, A.J., 2005. Ecosystem dynamics and export production in the central and eastern equatorial Pacific: a modeling study of impact of ENSO. *Geophysical Research Letter* 32, L2608.
- Wang, X., Christian, J.R., Murtugudde, R., Busalacchi, A.J., 2006. Spatial and temporal variability in new production in the equatorial Pacific during 1980–2003: physical and biogeochemical controls. *Deep Sea Research II* 53, 677–697.